Computers and Geosciences 123 (2019) 149–160

Contents lists available at ScienceDirect

Computers and Geosciences

journal homepage: www.elsevier.com/locate/cageo

Research paper

Modeling mafic carbonation efficiency using mafic rock chemistries from Nevada, USA

Daniel M. Sturmer[a,*,1], Regina N. Tempel[b,2], Jonathan G. Price[c,3]

[a] Department of Geology, University of Cincinnati, 500 Geology/Physics, PO Box 210013, Cincinnati, OH, 45221-0013, USA
[b] Department of Geological Sciences and Engineering, University of Nevada, Reno, 1664 N Virginia St., Reno, NV, 89557, USA
[c] Nevada Bureau of Mines and Geology, University of Nevada Reno, 1664 N Virginia St., Reno, NV, 89557, USA

ARTICLE INFO

Keywords:
Geology
Environmental science
Numerical environmental models

ABSTRACT

Mineral carbonation is one of the many ways that are being actively investigated to sequester point-source carbon dioxide emissions. However, relations between reaction conditions, variations in reactant mineral composition, and carbon sequestration potential are poorly understood. In this study we used reaction path geochemical modeling to evaluate carbon sequestration potential during ex-situ mineral carbonation of ten mafic rock samples from Nevada, USA. Models were run using arbitrary dissolution kinetics at temperatures between 0 and 200 °C. A subset of models were run using true dissolution kinetics. In the models, carbon is sequestered in 5 mineral phases: magnesite, siderite, dolomite, calcite, and dawsonite, with magnesite and dolomite the most abundant. Dawsonite sequesters carbon at T > 150 °C in most of the arbitrary kinetics models but is not a significant carbon sink in the models using true dissolution kinetics. The arbitrary kinetics models resulted in 4.5–13 mol of carbon sequestered per kg of reacted mafic rock. True kinetics models only resulted in 1–2 mol of carbon sequestered, but the models only reacted 12.5 to 15 wt percent of the mafic rock inputs. Product minerals using the arbitrary kinetics model have volumes 150%–470% larger than the reactant volumes, whereas using true kinetics the models have a modest increase. Modeling presented herein confirms several areas of Nevada as having potential for mafic rock carbonation, some of which are located near existing coal- and natural gas-fired power plants. As shown in this study, reaction path modeling is a vital and inexpensive tool to help optimize costs and reaction conditions for ex-situ mafic rock carbonation projects.

1. Introduction

Carbon dioxide is a greenhouse gas that acts to trap heat in the atmosphere. The amount of atmospheric CO_2 has been increasing from 278 ppm in the year 1750 (ice core estimate, Etheridge et al., 1996) to a global average of 405.0 ± 0.1 ppm in 2017 (Dlugokencky et al., 2018). The atmospheric CO_2 rate of increase has more recently been accelerating from 0.6 ± 0.1 ppm/yr in the 1960's to 2.3 ± 0.5 ppm/yr during the 2010's (Dlugokencky et al., 2018). Most of this observed change has been tied to combustion of fossil fuels, cement production, and changes in land use (Service, 2004; Hartmann et al., 2013; IPCC, 2014; Boden et al., 2017; Dlugokencky et al., 2018). This increase is projected to continue with an estimated 0.7% annual increase in global CO_2 emissions between 2015 and 2040 (EIA, 2017), with much of the increase coming from Asia, the Middle East, and Africa. One of the leading sources of the increase in atmospheric carbon is the burning of coal and natural gas for electricity production, and in the past few decades, both coal and natural gas have become the major source of electricity for Nevada, USA. Although carbon dioxide is released from these Nevada power plants every day, this carbon dioxide could potentially be captured and stored in the vast volumes of mafic rocks exposed in Nevada (Sturmer et al., 2007).

One of the recent foci of atmospheric greenhouse gas mitigation is capture, storage, and/or utilization of anthropogenically-produced carbon dioxide from point sources such as power and cement manufacturing plants (Dai et al., 2014, 2016; Ampomah et al., 2017; MacDowell et al., 2017; Rackley, 2017). Carbon capture from point source generators occurs by three main methods (Piers et al., 2011; Zhang et al., 2018a; b; c; d). The most common capture method occurs after combustion by scrubbing flue gas to capture CO_2. Several

* Corresponding author.
E-mail addresses: Daniel.Sturmer@uc.edu (D.M. Sturmer), gtempel@unr.edu (R.N. Tempel), jprice@unr.edu (J.G. Price).
[1] Built conceptual models, completed all modeling calculations, made figures, and wrote manuscript.
[2] Supervised geochemical modeling methods, revised and edited manuscript.
[3] Provided idea for project, revised and edited manuscript.

https://doi.org/10.1016/j.cageo.2018.12.003
Received 15 September 2018; Received in revised form 7 December 2018; Accepted 14 December 2018
Available online 15 December 2018
0098-3004/© 2018 Elsevier Ltd. All rights reserved.

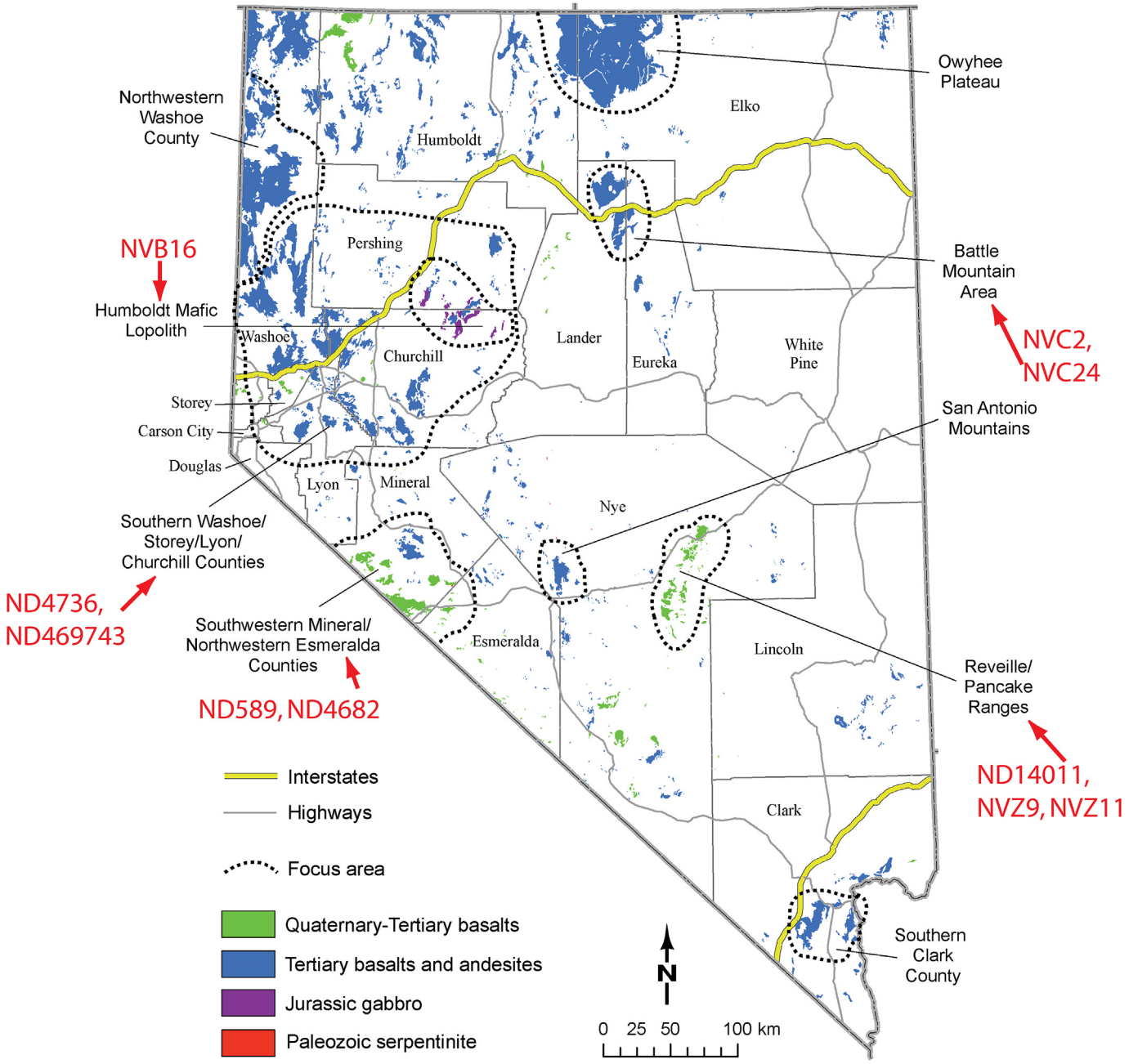

Fig. 1. Mafic rock outcrops in Nevada (modified from Sturmer et al., 2007; outcrop extents from Stewart and Carlson, 1978). Circled areas represent concentrations of mafic rocks large enough to supply at least one coal-fired power plant with material for carbon sequestration for 50 years (Sturmer et al., 2007). The ten samples modeled in this study come from these circled areas and are listed.

techniques have been investigated for scrubbing the flue gas, including adsorption, absorption, membranes, or combinations of these methods (Kim et al., 2012; Liu et al., 2014; Wang et al., 2017; Rezakazemi et al., 2017; Zhang et al., 2018c). The second method occurs during combustion, where pure O_2 is used instead of air as the primary oxidant in combustion, resulting in flue gas dominated by CO_2. Finally, CO_2 can be captured as part of the gasification process, prior to completion of fossil fuel combustion.

As a concentrated gas, CO_2 is hazardous because it is toxic to humans and heavier than the air so it preferentially hugs the ground. For example, ~80 million m^3 of carbon dioxide were expelled from Lake Nyos, Cameroon in 1986. The carbon dioxide flowed up to 25 km downhill into several villages, where ~1800 people died of asphyxiation (Krajick, 2003; Service, 2004). Therefore, most efforts to sequester carbon dioxide have focused on either injecting the CO_2 into the ground or sequestering the CO_2 in biomass. The main methods include enhanced oil recovery (EOR) (Dai et al., 2014, 2016; Ampomah et al., 2017; MacDowell et al., 2017), injection into deep saline aquifers, increasing biomass, and storage in mined caverns in salt formations (Price et al., 2005). Of these methods, EOR has been in use the longest (Middleton et al., 2012) with recent work (e.g., Dai et al., 2014, 2016; Ampomah et al., 2017) focusing on optimizing injection parameters to maximize CO_2 storage and oil production. However, scaling issues exist with global implementation of CO_2-EOR (Mac Dowell et al., 2017). Additionally, there are concerns around potential leakage of injected CO_2. For example, in a study of a system that was naturally leaking CO_2, Zhao et al. (2017) found plant development adversely affected when soil CO_2 concentrations rose above 10%.

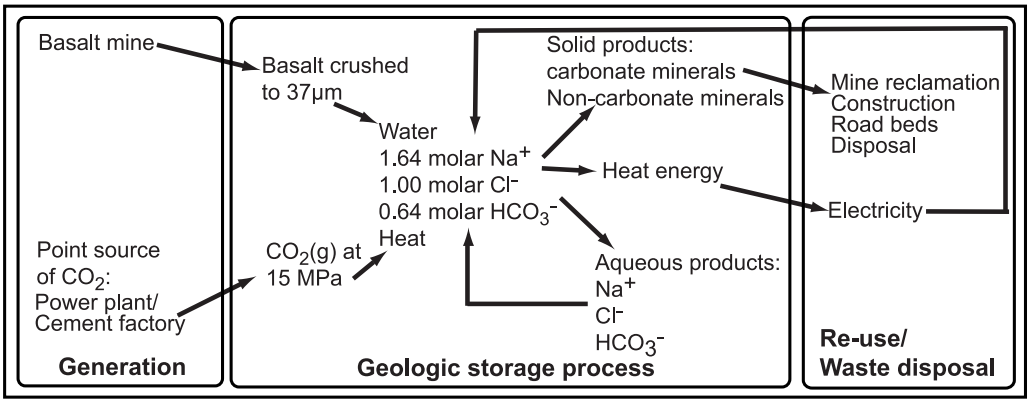

Fig. 2. Conceptual model for mafic rock carbonation. The model is based on the process for wet single-step carbonation of forsterite outlined by O'Connor et al. (2002, 2005) and Mazzotti et al. (2005). Note that many of the reactions are exothermic (Price et al., 2005; Sturmer et al., 2007).

One unconventional method of CO_2 sequestration that generally avoids the secondary release potential is mineral carbonation. In this process, CO_2 is reacted with Fe- and Mg-rich rocks and minerals or industrial waste products to form an inert product (Mazzotti et al., 2005; Price et al., 2005; Sturmer et al., 2007; Garcia et al., 2010; Gysi and Stefánsson, 2011, 2012a; 2012b; Aradóttir et al., 2012; Alfredsson et al., 2013; Galeczka et al., 2014; Johnson et al., 2014; Renforth et al., 2015; Rigopoulos et al., 2015, 2018; García del Real and Vishal, 2016; Guha Roy et al., 2016; McGrail et al., 2017; Adeoye et al., 2017; Griffioen, 2017; Snæbjörnsdóttir et al., 2017, 2018; Kularatne et al., 2018; Pan et al., 2018; Wolff-Boenisch and Galeczka, 2018). The reaction occurs naturally as a weathering reaction for mafic and ultramafic rocks. Many studies (see Mazzotti et al., 2005) have focused on reacting iron- and magnesium-bearing silicates (olivine, serpentine, orthopyroxene, clinopyroxene) with CO_2 to form iron, magnesium, and calcium carbonates (siderite, magnesite, dolomite, ankerite, calcite).

Several recent studies have focused on CO_2 injection into basalts in Iceland (Gislason et al., 2010; Alfredsson et al., 2013; Snæbjörnsdóttir et al., 2017, 2018) and Washington state (McGrail et al., 2014, 2017). These tests showed successful carbon sequestration over months to years, but also had occlusion of porosity by mineral precipitates. This pore space occlusion is due to precipitation of both carbonate and silicate reaction products. Depletion of divalent cations will lead to preferential precipitation of pore-filling clays (Wolff-Boenisch and Galeczka, 2018). However, this can be mitigated somewhat by controlling the fluid injection chemistry and injection flow rate (Wolff-Boenisch and Galeczka, 2018). There is also some concern over CO_2 injection and the potential for induced seismicity (Zoback and Gorelick, 2012), but this may be mitigated by mineral carbonation reducing fluid pressure following CO_2 injection into mafic rocks (Yarushina and Bercovici, 2013). Ultimately however, carbon sequestration potential for in-situ mineralization will be limited by the amount of reactive surface exposed to the fluids, which is a function of porosity and permeability of the mafic host rock.

Beginning in 2003, a coalition of western states, with funding from the U.S. Department of Energy, analyzed CO_2 sequestration potential in each state. Conventional methods of CO_2 sequestration studied included enhanced oil recovery, injection in deep saline aquifers, and biotic sequestration. These methods were rejected for Nevada, because Nevada does not have enough oil for enhanced oil recovery, it is illegal to inject any waste product into any aquifer, and Nevada does not have enough annual precipitation to support biotic sequestration (Price et al., 2005). The method with the most potential for Nevada is mineral carbonation of mafic rocks, which was explored in greater depth by Sturmer et al. (2007). That study evaluated the volume of mafic rock exposed in nine areas of the state for a large enough volume ($> 1.3\,km^3$) to supply a coal-fired powerplant with mafic rock feedstock for mineral carbonation for the life of the plant. Ultramafic rocks are thermodynamically more favorable for mineral carbonation but are relatively rare in Nevada (Fig. 1).

In this paper we present results from geochemical reaction path modeling of reactions between mafic rocks from Nevada and CO_2 from several of the areas considered by Sturmer et al. (2007). First, we discuss modeling parameters and assumptions, mafic rock geochemistry, and element partitioning with the models. Then critical parameters resulting from the models are discussed. These include differences between using arbitrary and true dissolution kinetics, assessments of mineral phases into which carbon is sequestered, relationships between mafic rock geochemistry and carbon sequestration potential, reaction temperature optimization, and volume ranges of product minerals. We then make the case for reaction path geochemical modeling as an integral tool for evaluating mafic rock carbonation projects.

2. Methods

The conceptual model is based on a successful experiment reacting forsterite (Mg-olivine) with carbon dioxide (Fig. 2, O'Connor et al., 2002, 2005; Mazzotti et al., 2005). By this procedure, forsterite is first mechanically ground to ~37 μm. The ground forsterite is dissolved in an aqueous solution of 1 M sodium chloride and 0.64 M sodium bicarbonate. The solution is then exposed to high-pressure carbon dioxide, and the forsterite is carbonated. When this reaction was conducted at 185 °C and a CO_2 partial pressure of 15 MPa, ~81% of the forsterite was carbonated in 1 h (O'Connor et al., 2005). The sodium and chloride ions in solution help to catalyze the reaction by releasing the metal cations from the forsterite, but most of those ions remain in solution after the reaction has completed and are thus recoverable. The reaction is optimized at different temperatures and CO_2 partial pressures for different minerals, but carbonation reactions are generally kept below 200 °C as CO_2 preferentially remains in the gas phase at higher temperatures (Mazzotti et al., 2005).

2.1. EQ3/6 model

All geochemical modeling in this study was done using the EQ3/6 code of Wolery (Wolery, 1992; Wolery and Daveler, 1992). EQ3/6 is a reaction path code that calculates aqueous speciation of water-rock reactions using sequences of thermodynamic equilibrium calculations. EQ3/6 is well-suited for this study because it has a large geochemical reference database, the ability to model kinetics, and a variety of activity coefficient models at the range of temperatures of interest for this study (Crawford, 1999). For this study EQ3/6 was used to simulate reaction of 10 mafic rock samples from Nevada and an "average basalt" with CO_2 in an aqueous system using arbitrary dissolution kinetics (Table 1). The 10 samples are from the PETROS and NAVDAT online databases of published igneous rock geochemical data (Table 1) and all

Table 1
Geochemical samples used in this study. Data were retrieved from NAVDAT (nd samples; http://navdat.kgs.ku.edu/) and PETROS (nv samples, http://www.ngdc.noaa.gov/mgg/geology/petros.html) databases.

Sample	Location	County	Latitude	Longitude	Reference
hypbas	n/a	n/a	n/a	n/a	Sturmer et al. (2007)
nd589	SW Mineral County	Mineral	38.1733	−118.6466	Brem (1978)
nd4682	Garfield Hills	Mineral	38.4833	−118.35	Ormerod (1988)
nd4736	Pah Rah Range	Washoe	39.5333	−119.7	Ormerod (1988)
nd14011	S. Pancake Range	Nye	38.2	−116.1	Lum et al. (1989)
nd469743	Pah Rah Range	Washoe	39.488	−119.618	Everson (1979)
nvb16	W. Humboldt Range	Pershing	40	−118	Speed (1962)
nvc2	Battle Mountain	Lander	41	−117	Roberts (1964)
nvc24	Sheep Creek Range	Lander	41	−117	Mark et al. (1975)
nvz9	Lunar Crater Area	Nye	38	−116	Trask (1969)
nvz11	Lunar Crater Area	Nye	39	−116	Wilshire et al. (1972)

sample names are from the databases. Samples with the most mafic values were chosen for each of the geographic areas of interest (Fig. 1). The aqueous solution (with sodium bicarbonate and sodium chloride) was first modeled, and then the reaction of mineral inputs with CO_2 and the aqueous solution were modeled. A subset of three mafic rock chemistries were analyzed using true dissolution kinetics.

2.2. Assumptions

The EQ3 input files (Wolery, 1992) consisted mainly of the added sodium chloride and sodium carbonate. Each of these species was assumed to completely dissociate, so that Na^+, Cl^-, and HCO_3^- were added at concentrations of 1.64, 1.00, and 0.64 mol per liter, respectively. This assumption may not be valid; however, it was acceptable to simplify the model. Initial neutral pH was assumed. To prevent error messages when running the model in EQ6 (Wolery and Daveler, 1992), any ions that were part of the minerals added in EQ6 were added at an arbitrary trace amount (1×10^{-8} mol/liter) to the EQ3 input file. Activity coefficients were calculated using the B-dot version of the Debye-Hückel equation. Corundum was suppressed as it is stable above 450 °C (Deer et al., 1966) and all analyses for this study were between 0 and 200 °C.

For each run in EQ6, a total of 1 kg of normative minerals from each of the 11 samples was added as solid reactants. Moles of minerals added were calculated based on CIPW norms calculated from major oxide geochemical data (Table 2). CIPW norms were calculated using the CIPW-norm calculator from the Saskatchewan isotope laboratory (available free for academic use at http://sil.usask.ca/software.htm). Reactant minerals are assumed to be distinct, mechanically separable phases. A closed system was assumed, and solid solutions were not considered. Carbon dioxide was added to the system using the fixed fugacity option to fix CO_2 fugacity at 150 bar (15 MPa) and allow up to 10 mol of CO_2 to be added. Models were calculated at 25 °C steps, between 0 °C and 200 °C. Higher temperatures were not considered as CO_2 preferentially remains a gas above 200 °C (Mazzotti et al., 2005). Pressure was set from the data file reference pressure curve. All arbitrary kinetics water-rock interactions were calculated using the relative rate and partial equilibrium equations for the forward and reverse reactions, respectively.

A subset of the samples was rerun using true dissolution kinetics. Kinetics values (Table 3) were obtained from Brantley (2003). For runs with kinetics, reactant surface area must be provided. Total surface area of each reactant was calculated assuming that the sample had been crushed into 37 μm-diameter spheres following the conceptual model (O'Connor et al., 2002, 2005; Mazzotti et al., 2005).

3. Results

Model results have carbon sequestered in several Fe, Mg, Na, Ca, and Al-bearing mineral phases. Each model also has non-carbon-bearing product minerals. A sample model output is presented in Fig. 3, showing minerals precipitated throughout the model. Each of these elements is a component of the input mafic rock minerals. Partitioning of each of these cations and comparison with observations from published experimental work is discussed below.

3.1. Magnesium

Magnesium is one of the more critical elements for sequestering carbon. Dolomite and magnesite are ubiquitous product minerals for all arbitrary kinetics models and most true kinetics models. The exceptions in the true kinetic models include a lack of dolomite precipitation at low temperatures, at $T > 50$ °C for sample nvz11, and suppression of magnesite precipitation at $T > 150$ °C by calcite and dawsonite for sample nd467943. Mg was also present in nontronite-Mg (Mg-smectite) in the arbitrary kinetics models. Nontronite-Mg is generally present at temperatures between 50 and 100 °C, replacing nontronite-K, which precipitates at lower temperatures, and replaced by nontronite-Na,

Table 2
CIPW norms for samples used in this study.

Sample	Forsterite Mg_2SiO_4	Fayalite Fe_2SiO_4	Wollastonite $CaSiO_3$	Enstatite $MgSiO_3$	Ferrosilite $FeSiO_3$	Anorthite $CaAl_2Si_2O_8$	Albite $NaAlSi_3O_8$	Orthoclase $KAlSi_3O_8$	Nepheline $NaAlSiO_4$	Magnetite Fe_3O_4	Hematite Fe_2O_3
hypbas	15.00	5.00	7.00	23.00	1.00	3.00	1.00	0.00	0.00	0.00	0.00
nd589	9.46	0.00	8.06	12.57	2.61	23.15	26.59	7.72	0.00	9.85	0.00
nd4682	13.18	0.00	7.18	10.74	0.00	25.25	28.40	8.36	0.00	0.00	6.89
nd4736	12.68	0.00	5.90	8.18	0.00	27.54	28.01	11.05	0.00	0.00	6.63
nd14011	15.96	9.74	8.00	4.97	3.03	24.76	27.46	6.08	0.00	0.00	0.00
nd469743	12.00	3.23	9.67	8.36	0.00	26.10	28.98	11.66	0.00	0.00	0.00
nvb16	33.38	3.96	4.99	18.65	2.21	19.14	12.95	2.14	0.00	2.59	0.00
nvc2	14.03	5.07	5.80	5.13	0.00	28.59	34.67	6.71	0.00	0.00	0.00
nvc24	10.17	4.04	8.17	13.72	4.40	37.34	20.04	2.13	0.00	0.00	0.00
nvz9	13.12	4.67	12.58	9.28	0.00	21.01	9.23	11.79	18.31	0.00	0.00
nvz11	79.63	7.51	0.00	9.86	0.00	3.00	0.00	0.00	0.00	0.00	0.00

Table 3
Log dissolution rates and activation energies used for true dissolution kinetics models. All values from Brantley (2003).

Mineral	Formula	Log dissolution rate (mol/m^2/s)	Activation energy (kcal/mol)
Forsterite	Mg_2SiO_4	−9.4	19
Fayalite	Fe_2SiO_4	−9.4	19
Wollastonite	$CaSiO_3$	−7.8	13
Enstatite	$MgSiO_3$	−10.5	12
Anorthite	$CaAl_2Si_2O_8$	−11.4	19
Albite	$NaAlSi_3O_8$	−12.2	16
K-Feldspar	$KAlSi_3O_8$	−12.4	13

which precipitates at higher temperatures. True kinetics models only had precipitation of nontronite-Na.

3.2. Iron

Iron is present in one carbon-bearing and several non-carbon-bearing product minerals. Siderite is a product mineral at all temperatures for all true kinetic samples and all arbitrary kinetic samples except nd4682 and nd4736. This may be due to a lack of normative fayalite (the Fe-end member of olivine) in the CIPW norms for these samples. Iron is present in the three nontronite species, which are present in all models at T≤°175C. Iron is also in hematite, which is present in all models at T = 200 °C and at all temperatures for sample nvz11 using true kinetics.

3.3. Aluminum and Sodium

Aluminum and Sodium are present in one carbon-sequestering and several non-carbon sequestering product minerals. These elements are present in dawsonite, which is a hydrated sodium aluminum carbonate. Dawsontie precipitated in arbitrary kinetics and two true kinetics models for all samples at T < 150 °C. Dawsonite formed early in the true kinetics models for sample nvz11, but it was replaced by nontronite-Na later in the reaction. For all samples at T ≥ 150 °C, albite forms instead of dawsonite. The loss of the carbon-bearing mineral phase dawsonite is displayed by the decrease in moles of carbon sequestered for most samples between 125 °C and 150 °C (Figs. 4 and 5). Sodium and aluminum are present in product minerals albite and nontronite-Na. In addition, aluminum is also present in nontronite-Mg, nontronite-K, microcline, muscovite, and diaspore, all of which are non-carbon-bearing product minerals.

3.4. Calcium

Calcium is present in two carbon-sequestering product minerals. Dolomite is present as a product mineral for all models using both arbitrary and true kinetics. Calcite only precipitates for the true kinetics models of sample nd467943 at T ≤ 125 °C. Calcium is not present is any other product minerals for this set of models.

3.5. Product mineral comparison

All carbon-bearing product minerals reported in these models have been observed in experimental and/or natural reactions of mafic rocks with CO_2. Magnesite is a common product mineral in experimental carbonation of mafic rocks (Rogers et al., 2006; Garcia et al., 2010; Johnson et al., 2014; Sissman et al., 2014; Kularatne et al., 2018). Siderite is also present in some experimental products and natural systems (Rogers et al., 2006). Mg- and Fe-bearing carbonates are especially prevalent due to the relative instability of olivine at surface (or near-surface) conditions (García del Real and Vishal, 2016). Calcite and dolomite have been observed as product minerals in lab experiments (Aradóttir et al., 2012; Gysi and Stefánsson, 2012b; Guha Roy et al., 2016; Wolff-Boenisch and Galeczka, 2018), well injection experiments (Snæbjörnsdóttir et al., 2017), and in natural systems (Rogers et al., 2006). Dawsonite is generally over-reported in models (Wolff-Boenisch and Galeczka, 2018) but has been observed to precipitate with a supply of Na + cations and continuous CO_2 partial pressure (Hellevang et al., 2011, 2014). End-member carbon-bearing phases were used for calculations in these models, but solid-substitutions are commonly reported from experimental studies, including ankerite (Ca(Fe, Mg, Mn) $(CO_3)_2$) (Gysi and Stefánsson, 2012b; McGrail et al., 2017), Fe-bearing magnesite (Kularatne et al., 2018), and Fe-Mg carbonates (Aradóttir, 2012; Gysi and Stefánsson, 2012a; Snæbjörnsdóttir et al., 2018).

Most of the non-carbon-bearing secondary minerals that precipitate in the models have been observed in experimental studies or natural analogue systems. Smectite is a common secondary product in experimental mafic carbonation reactions (Aradóttir et al., 2012; Gysi and Stefánsson, 2012a, 2012b; Guha Roy et al., 2016; Snæbjörnsdóttir et al., 2018; Wolff-Boenisch and Galeczka, 2018). Though specific clays are generally not identified, nontronite has been identified as the main smectite clay in some studies (Gysi and Stefánsson, 2012a; Hellevang et al., 2017). Aluminum and iron oxides, hydroxides, and oxy-hydroxides, including hematite, are common secondary minerals in experimental mafic carbonation reactions (Aradóttir et al., 2012; Gysi and Stefánsson, 2012a; Kularatne et al., 2018; Snæbjörnsdóttir et al., 2018), particularly when the experiments are done at temperatures above ~150 °C (Gysi and Stefánsson, 2012b). Albite and phyllosilicates (including chlorite but not muscovite) have been observed from higher-temperature experiments (Gysi and Stefánsson, 2012b; Kularatne et al., 2018). Microcline is not known to have been reported as a product mineral of mafic carbonation experiments, with Na^+ and Al^{3+} cations likely partitioned into clays and/or zeolites.

4. Discussion

4.1. Arbitrary and true dissolution kinetics

More carbon was sequestered using the arbitrary kinetic reaction path than the true kinetic path. Arbitrary kinetic models were run for all rocks (Fig. 4), and true kinetics models were run for three of the mafic rock samples (Fig. 5). The true kinetics models for all samples sequestered between 1 and 2 mol C/kg reactant by the end of the reaction path. Using arbitrary kinetics, 4.5–7 mol C/kg reactant were sequestered for samples nd469743 and nvc2, and ~13 mol C/kg reactant were sequestered for sample nvz11.

Percent reactant mineral dissolution is the main cause of the difference in carbon sequestration between the two kinetics options. Using the arbitrary reaction path, the reactant minerals are forced to dissolve completely, thereby placing a constant stream of cations in solution to form carbonate minerals. The true kinetics option does not force the reactants to dissolve completely; rather the solid reactants dissolve at the true kinetic rate until they establish equilibrium with the solution. The amount of dissolution is also a function of surface area, with dissolution increasing as surface area increases. For these models, only ~120–145 g of the initial input kilogram dissolve, with ~90% (130 g) of the dissolution from forsterite. The decrease in the amount of reactant dissolved results in a decrease in metal cations released and available to bond with carbonate anions.

Carbon sequestration efficiency is generally greater using true dissolution kinetics when compared on a carbon sequestered per kg of reactant dissolved basis. Using this metric, samples nd469743 and nvc2 sequester between 8 and ~12 mol C per kg sample reacted, compared with 4.5–7 mol C for arbitrary kinetics. Sample nvz11 results in slightly more carbon sequestered per kg dissolved with true dissolution kinetics, except for at lower temperatures (Fig. 5).

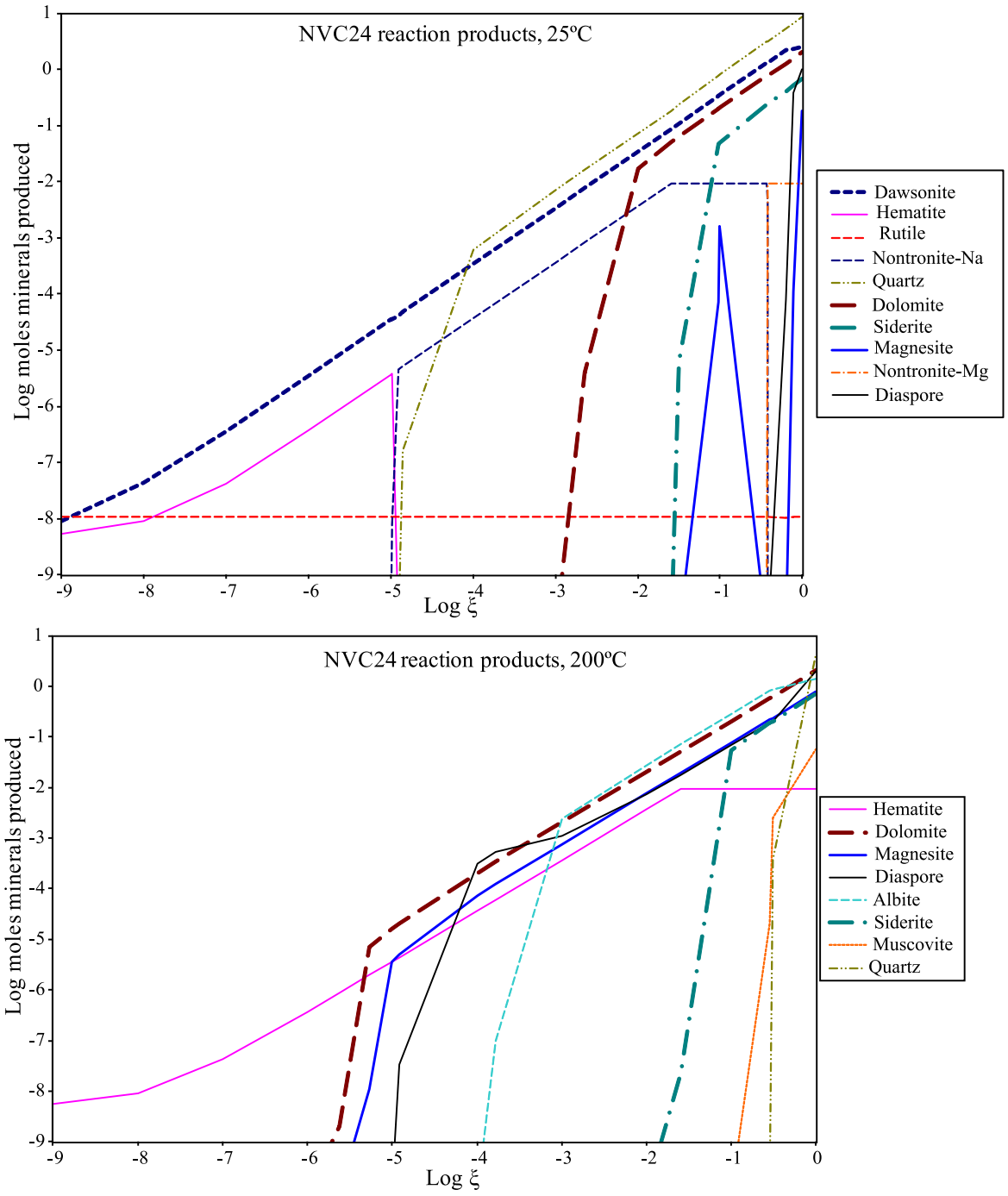

Fig. 3. Examples of product minerals formed during low-temperature (25 °C) and high-temperature (200 °C) reactions for nvc24. Log product minerals are plotted against log ξ (ξ is a modeling parameter where ξ = 0 represents reaction initiation and ξ = 1 represents reaction completion, in this case dissolution of all reactant minerals).

4.2. Cation partitioning and carbon sequestration

Mg and Ca are the most critical cations for carbon sequestration when modeled using arbitrary kinetics. Mg results in 30–70% of the carbon sequestered for most of the models. The percentage of carbon captured in Mg-bearing minerals increases with increasing temperature. Sample nvz11 has 88–94% of the carbon sequestered in Mg-bearing minerals. For most of the samples 20–40% of the carbon is captured in Ca-bearing minerals. Na and Al (cations in dawsonite) are important at lower temperatures, capturing 20–45% of the carbon at 0 °C and 25 °C. At higher temperatures the importance of Na + Al for carbon capture decreases to 10–30% at 125 °C. At T ≥ 150 °C dawsonite is not stable and Na + Al do not participate in carbon capture. Fe accounts for less than 15% of the carbon captured for most of the models. The prevalence of Mg- and Ca-bearing minerals for carbon sequestration is consistent with observations from lab experiments (Garcia et al., 2010; Aradóttir et al., 2012; Gysi and Stefánsson, 2012b; Sissman et al., 2014; Johnson et al., 2014; Guha Roy et al., 2016; Wolff-Boenisch and Galeczka, 2018), field-scale tests (Snæbjörnsdóttir et al., 2017; McGrail et al., 2017; Kularatne et al., 2018), and natural systems (Rogers et al., 2006).

Ca and Mg are the critical cations for carbon sequestration using true dissolution kinetics. For sample nvz11, 94–96% of the carbon is sequestered as magnesite. For nvc2, 43–68% of carbon is stores in

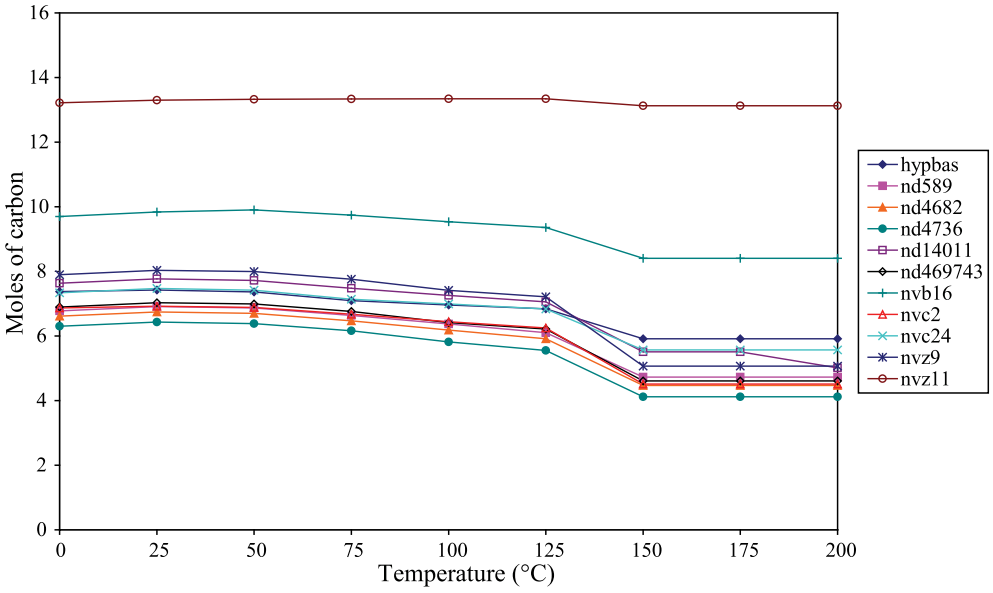

Fig. 4. Moles of carbon sequestered per kg of reacted basalt as a function of temperature using arbitrary dissolution kinetics. Above 150 °C dawsonite is not stable and albite precipitates instead, resulting in a drop of 1.5–3 mol of carbon sequestered per kg of basalt reacted. Dawsonite is a relatively minor component in the product mineralogy of sample nvz11 making this sample less sensitive to higher temperature reactions.

magnesite (Mg) and dolomite (Mg + Ca). The amount of dolomite precipitated decreases with temperature, so Ca decreases from 43% to 15% of carbon captured. Sample nd469743 has calcite precipitating at lower temperatures, so Ca is responsible for 74% of carbon capture at 0 °C, decreasing to 27% at 200 °C. Mg increases from 24% of carbon capture at 0 °C to 62% at 200 °C, reflecting the loss of calcite as a precipitated mineral and increases in the amounts of dolomite and magnesite precipitated. Fe is responsible for between 1 and 17% of the carbon captured, increasing in importance with increasing temperature. Na and Al are not important cations for carbon sequestration in the true dissolution kinetics models as dawsonite accounts for < 2% of carbon sequestration.

4.3. Mafic rock geochemistry and carbon sequestration

The geochemistry of the mafic rock used in mafic rock carbonation has a large impact on both the carbon sequestration potential and the volume of product minerals following mafic carbonation reactions. In general, volcanic rocks lower in SiO_2 and higher in Fe and Mg have greater potential for sequestering CO_2 with ultramafic rocks having the highest sequestration potential (García del Real and Vishal, 2016). In Nevada, ultramafic rocks are volumetrically minor, but mafic rocks are abundant (Stewart and Carlson, 1978; Sturmer et al., 2007). The anomalous sample in these models (nvz11) is a lherzolite, an ultramafic rock from a xenolith in basalt. Using arbitrary kinetics, the maximum moles of C sequestered ranges between 6.5 and 8 mol of C sequestered per kg reacted, with an increase to 8–13 mol of C sequestered where SiO_2 content drops below 46% (Fig. 6).

The Fe/Mg ratio also appears to affect the carbon sequestration potential of mafic rocks (Fig. 7). For the samples from Nevada, increased carbon sequestration correlated with increasing percent normative forsterite, which is the Mg-bearing end member of olivine. This was also true in models using true dissolution kinetics.

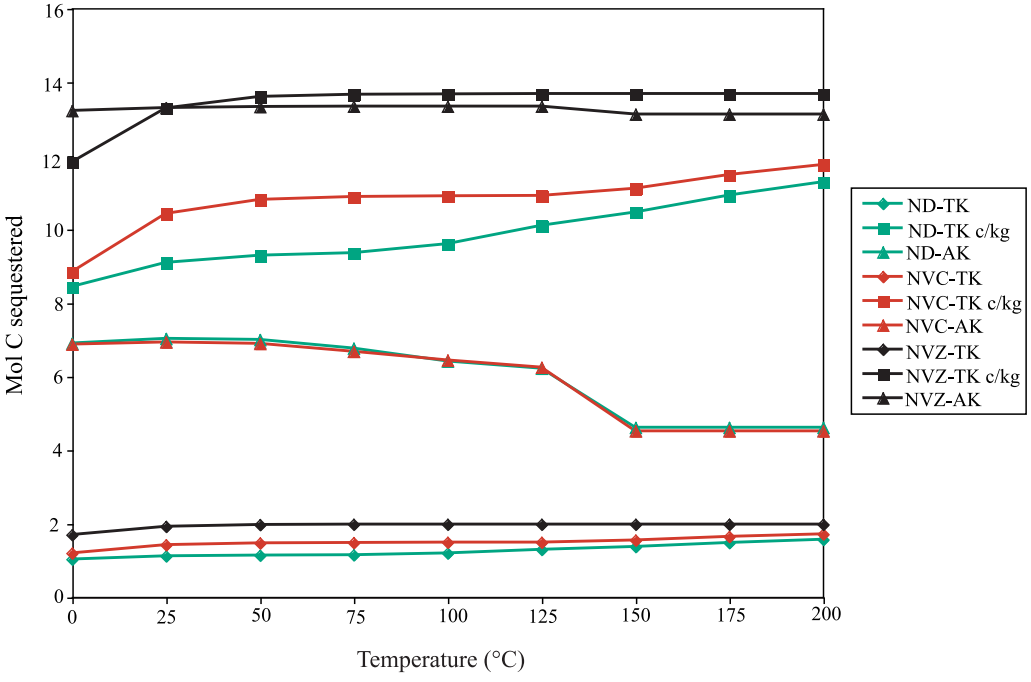

Fig. 5. Graph showing the amounts of carbon sequestered using true dissolution kinetics to reaction completion (diamonds), arbitrary dissolution kinetics per kg of mafic rock dissolved (triangles), and true dissolution kinetics per kg of mafic rock dissolved (squares) for samples nd469743 (green), nvc2 (red), and nvz11 (black). (For interpretation of the references to colour in this figure legend, the reader is referred to the Web version of this article.)

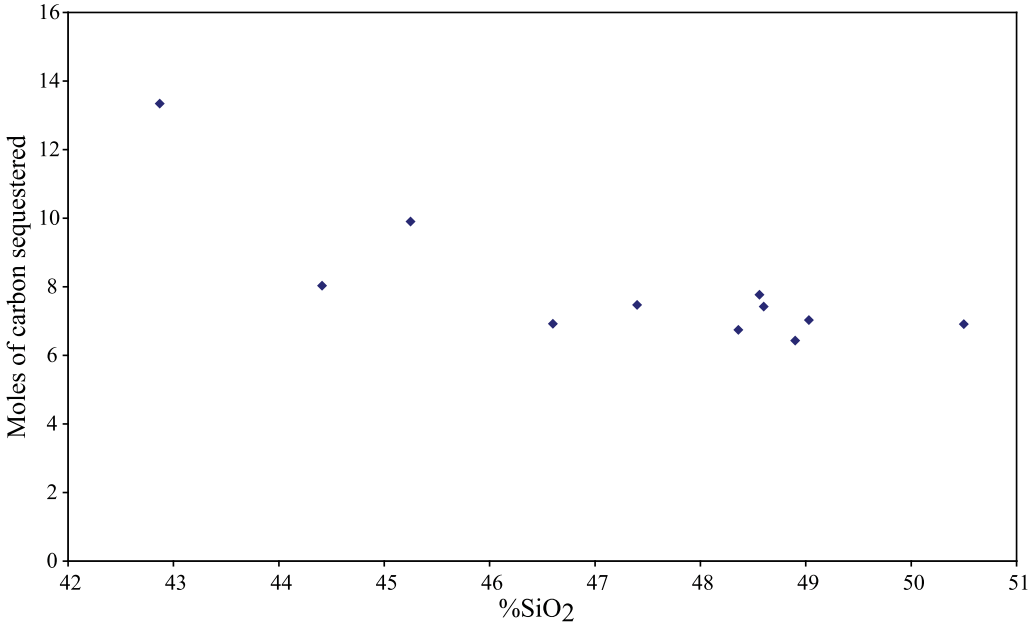

Fig. 6. Maximum moles of carbon sequestered per kg of reacted basalt plotted against percent SiO_2.

4.4. Optimizing reaction temperature to maximize carbon sequestration

In the arbitrary kinetics models, most mafic rock samples have carbon sequestration maxima with the reaction at 25 °C (Fig. 4). The exceptions are the picrite cumulate (nvb16; sequestration maximum at 50 °C) and the lherzolite xenolith (nvz11; maximum at 100–125 °C). The models are insensitive to reaction temperature below ~100 °C. Above 150 °C dawsonite is not stable and albite precipitates instead, resulting in a drop of 1.5–3 mol of carbon sequestered per kg of basalt reacted. Dawsonite is a relatively minor component in the product mineralogy of sample nvz11, as this sample only has 0.16 wt percent Na_2O compared to 1.5–4% for the other samples. Therefore, low sodium content in the mafic rock decreases reaction sensitivity to temperature.

True dissolution kinetics results show a more efficient sequestration of carbon per unit volume, but less sequestration at modeled reaction completion (Fig. 5). Using true kinetics, reactions reached completion at 12–14.5% mineral dissolution, compared to 100% dissolution for the arbitrary models. This results in only ~1.5–2 mol of C sequestered at reaction completion compared to the arbitrary dissolution kinetics with ~5–13 mol C sequestered. However, when the two methods are compared per kg of mafic rock reacted, the true kinetic reactions result in more carbon sequestration. Sample nvz11 results in a slight increase in CO_2 sequestered, whereas nvc2 and nd469743 have an increase of between 20 and 140% (Fig. 5). The gap in carbon sequestration efficiency increases with increasing temperature. This is dominantly due to increased dissolution of forsterite and fayalite with increasing temperature in the true dissolution kinetics models.

The other element to consider is time. Reaction rates increase with increasing temperature (Fig. 8). Reaction completion takes several years at 25 °C, down to less than an hour at 175–200 °C. This supports the study of O'Connor et al. (2002) where they allowed the mafic

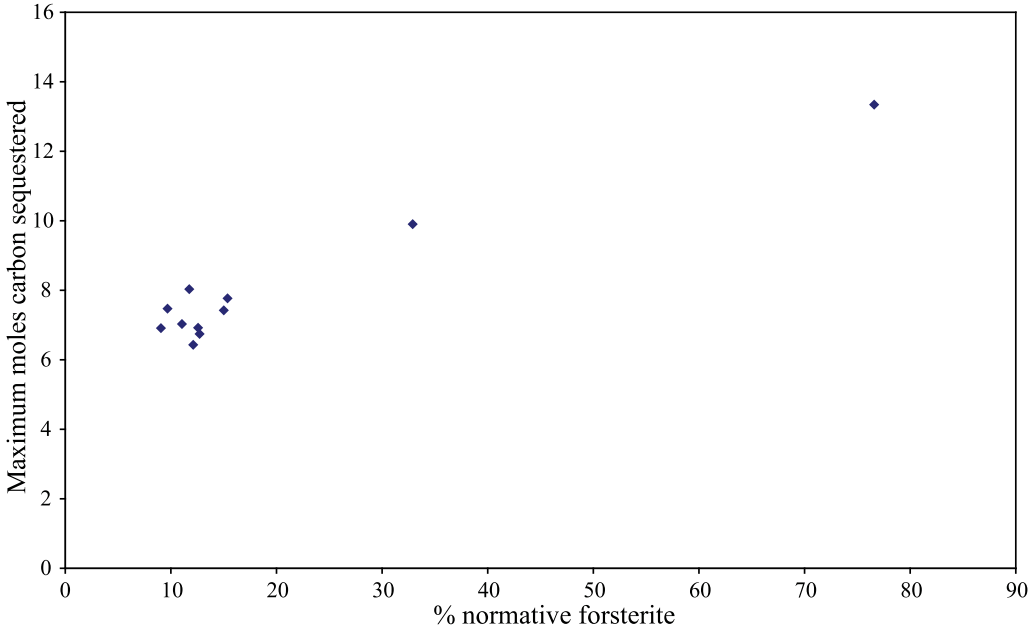

Fig. 7. Maximum moles of carbon sequestered per kg of reacted basalt plotted against percent normative forsterite.

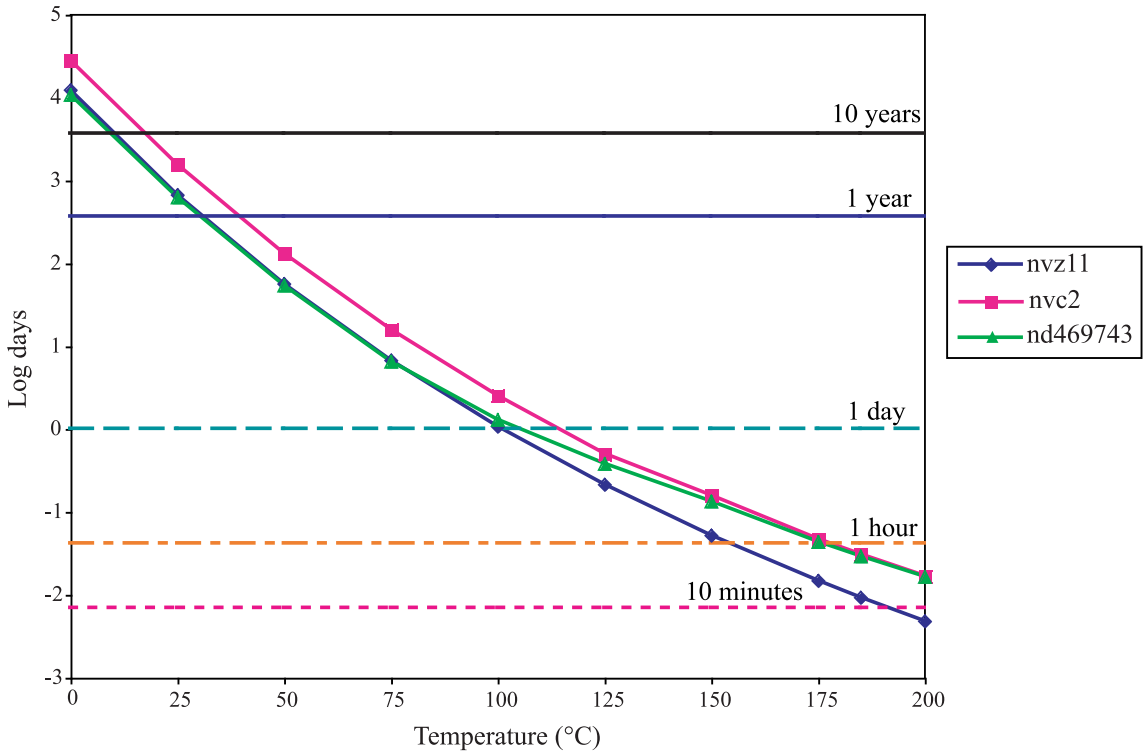

Fig. 8. Relationship of reaction rate to temperature. O'Connor et al. (2002) allowed the forsterite-carbon dioxide reaction to run for 1 h. The only reactions that reach completion in this time frame are those at or above 175 °C.

carbonation reaction to go to completion within 1 h at 185 °C. The carbonation reactions are dominantly exothermic, which may decrease the initial amount of energy input for an individual batch reaction. Ultimately, maximum carbon sequestration will occur at higher temperatures, but ideal temperature for an individual reactor will depend on set up, availability rate of mafic rock and CO_2, and economic factors.

4.5. Product volume optimization

One of the challenges with ex-situ mineral carbonation reactions is that the volume of product minerals is larger than the volume of reactant minerals (Fig. 9). All volumes were calculated using an average 20% porosity, though that value could vary. With arbitrary reaction kinetics, low temperature reactions produce 3–5 times as much product volume as the high temperature reactions for all samples but nvz11 (the lherzolite). The volume increase is mainly a function of dawsonite precipitation. Dawsonite is most abundant as a product in the low temperature reactions and has a molecular volume of ~500 cm^3/mol; 3.5 to 28 times larger than the other product minerals. Therefore, at lower temperatures product volumes are much higher. At higher temperatures the volume increase of product minerals is lower, but less carbon is sequestered as albite precipitates instead of dawsonite at T ≥ 150 °C.

The true kinetics models result in a lower volume increase per kg of reactant. In these models only ~12–14.5% of the reactants dissolve at model completion/equilibrium, resulting in a volume loss of between 14 and 25%. When calculated adding 20% porosity, the combined product and unused reactant minerals result in a 12%–39% increase in volume across the temperature range modeled (Fig. 10). This is a much lower increase than the 150%–470% volume increase at low temperatures in the arbitrary kinetics models, due to the relatively minimal precipitation of dawsonite in the true kinetics models.

4.6. Modeling use for mafic carbonation

Reaction path geochemical modeling can be very valuable when assessing a mafic carbonation project. Running a series of models can help to choose between potential mafic rock source materials, optimize reaction conditions, and predict how much product will result from the reactions. These are critical for choices in locating and designing facilities, estimating costs, and project viability.

This study demonstrates the utility of reaction path geochemical modeling for making informed decisions when choosing between potential sites for CO_2 sequestration by mafic carbonation. However, other economic factors must be considered when ranking potential sequestration sites. For example, of the samples considered in this study, a sample from the Reveille/Pancake Range area (Fig. 1) sequesters the most carbon per kg of rock reacted (Fig. 4). However, these rocks are located far from infrastructure and potential CO_2 point sources. The nearest coal-fired power plant is at Valmy (280 km to the north-northwest), and the nearest natural gas power plants are in northern Clark County (250 km south-southeast) and in Lyon County (300 km west) (Fig. 1, NV Energy, 2018). In this case it would likely be more cost effective to choose a basalt field near power plant even if the amount of carbon sequestered per kg of rock reacted is lower. For example, the Battle Mountain area basalt field is only 30 km from the Valmy coal-fired power plant (Fig. 1). Additionally, reaction path modeling provides an estimated range of product materials following the mineral carbonation reactions. The product materials could possibly be sold for aggregate feedstock, thereby increasing the economic viability of mineral carbonation and helping to alleviate the ever-increasing demand for aggregate used in construction and land reclamation (e.g., Peduzzi, 2014). Recent work has also shown the potential to generate and capture H_2 as a byproduct of mafic rock carbonation (Kularatne et al., 2018). The hydrogen is produced by oxidation of iron in olivine during the carbonation reactions. As shown here, the estimates produced by reaction path geochemical modeling are a relatively quick and inexpensive way to estimate both carbon sequestration potential and

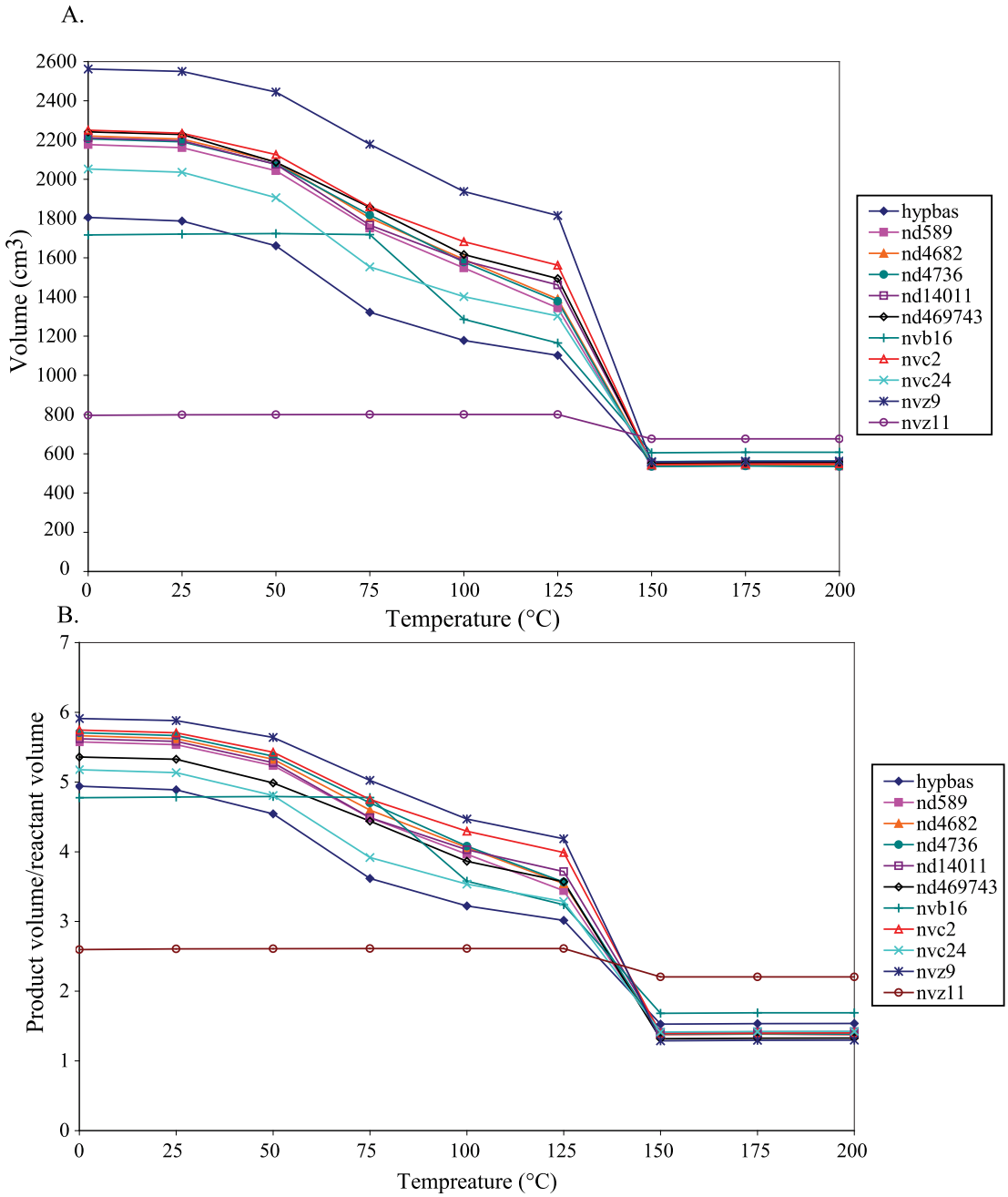

Fig. 9. A. Volume of solid product minerals (assuming 20% porosity) versus reaction temperature. The volume increase at lower temperatures is mainly a function of dawsonite precipitation. B. Ratio of solid product (assuming 20% porosity) and solid reactant plotted against reaction temperature.

amounts of product material when assessing the economic feasibility of a proposed mineral carbonation project.

5. Conclusions

Reaction path geochemical modeling of mafic rock-CO_2 reactions of mafic rocks from Nevada results in carbon being sequestered in up to five mineral phases: magnesite, dolomite, calcite, siderite, and dawsonite. Using arbitrary dissolution kinetics, the samples sequester between 4.5 and 13 mol of carbon per kg of mafic rock. The product minerals in these models have a much larger volume than the reactants, though the volume differential decreases with increasing temperature and decreasing precipitation of dawsonite. Models using true dissolution kinetics only resulted in 1–2 mol of carbon sequestered per kg of reactant, but the models only allowed 12.5–15% of the mafic rock to react. However, the sequestration is more efficient on a per-kg-reacted basis. The results of this and further geochemical modeling will help both to elucidate the geochemical processes involved in mineral carbonation and to optimize conditions for ex-situ mineral carbonation. With more research and physical experimentation, mineral carbonation has the potential to drastically reduce the amount of carbon dioxide released from point sources in areas like Nevada, where more conventional sequestration methods are not possible.

Declaration of interest

None.

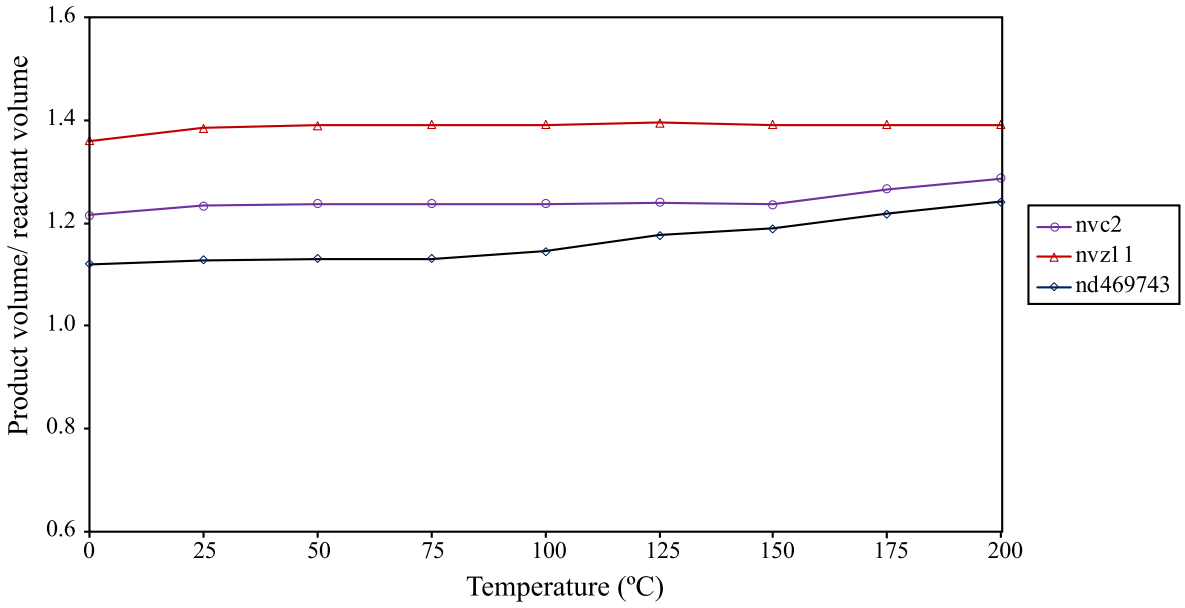

Fig. 10. Ratio of solid product (assuming 20% porosity) and solid reactant plotted against temperature for true kinetics models.

Acknowledgments

The authors thank Reza Soltanian for the invitation to submit this work to this special issue. Thanks also go to Thomas J. Wolery and Stephanie A. Daveler for access to the EQ3/6 program. This work was initiated following completion of work on the possibility of mafic carbonation in Nevada funded by the U.S. Department of Energy. However, this research did not receive any grant from funding agencies in the public, commercial, or not-for-profit sectors.

References

O'Connor, W.K., Dahlin, D.C., Rush, G.E., Dahlin, C.L., Collins, W.K., 2002. Carbon dioxide sequestration by direct mineral carbonation: process mineralogy of feed and products. Miner. Metall. Process. 19 (2), 95–101.

O'Connor, W.K., Dahlin, D.C., Rush, G.E., Gedermann, S.J., Penner, L.R., Nilsen, D.N., 2005. Aqueous mineral carbonation, final report. Department of Energy, DOE/ARC-TR-04-002.

Adeoye, J.T., Menefee, A.H., Xiong, W., Wells, R.K., Skemer, P., Giammar, D.E., Ellis, B.R., 2017. Effect of transport limitations and fluid properties on reaction products in fractures of unaltered and serpentinized basalt exposed to high P_{CO2} fluids. International Journal of Greenhouse Gas Control 63, 310–320. https://doi.org/j.ijggc.2017.06.003.

Alfredsson, H.A., Oelkers, E.H., Hardarsson, B.S., Franzson, H., Gunnlaugsson, E., Gislason, S.R., 2013. The geology and water chemistry of the Hellisheidi, SW-Iceland carbon storage site. International Journal of Greenhouse Gas Control 12, 399–418. https://doi.org/10.1016/j.ijggc.2012.11.019.

Ampomah, W., Balch, R.S., Cather, M., Will, R., Gunda, D., Dai, Z., Soltanian, M.R., 2017. Optimum design of CO_2 storage and oil recovery under geological uncertainty. Appl. Energy 195, 80–92. https://doi.org/10.1016/j.apenergy.2017.03.017.

Aradóttir, E.S.P., Sonnenthal, E.L., Jónsson, H., 2012. Development and evaluation of a thermodynamic dataset for phases of interest in CO_2 mineral sequestration in basaltic rocks. Chem. Geol. 304–305, 26–38. https://doi.org/10.1016/j.chemgeo.2012.01.031.

Boden, T.A., Andres, R.J., Marland, G., 2017. Global, regional, and national fossil-fuel CO_2 emissions: Carbon Dioxide Information Analysis Center. Oak Ridge National Laboratory. http://doi.org/10.3334/CDIAC/00001_V2017.

Brantley, S.L., 2003. Reaction kinetics of primary rock-forming minerals under ambient conditions. Treatise on Geochemistry 5, 73–117.

Brem, G.F., 1978. Petrogenesis of late Tertiary potassic volcanic rocks in the Sierra Nevada and western Great Basin. Ph.D. dissertation. University of California, Riverside, pp. 351.

Crawford, J., 1999. Geochemical modelling – a review of current capabilities and future directions: Stockholm 262. Swedish Environmental Protection Agency, SNV Report, pp. 39.

Dai, Z., Middleton, R., Viswanathan, H., Fessenden-Rahn, J., Bauman, J., Pawar, R., Lee, S.-Y., McPherson, B., 2014. An integrated framework for optimizing CO_2 sequestration and enhanced oil recovery. Environ. Sci. Technol. Lett. 1, 49–54. https://doi.org/10.1021/ez4001033.

Dai, Z., Viswanathan, H., Middleton, R., Pan, F., Ampomah, W., Yang, C., Jia, W., Xiao, T., Lee, S.-Y., McPherson, B., Balch, R., Grigg, R., White, M., 2016. CO_2 accounting and risk analysis for CO_2 sequestration at enhanced oil recovery sites. Environ. Sci. Technol. 50, 7546–7554. https://doi.org/10.1021/acs.est.6b01744.

Deer, W.A., Howie, R.A., Zussman, J., 1966. An introduction to the rock-forming minerals. John Wiley and Sons, New York, pp. 528.

Dlugokencky, E.J., Hall, B.D., Montzka, S.A., Dutton, G., Mühle, J., Elkins, J.W., 2018. Atmospheric composition. In: In: Dunn, R.J.H., Stanitski, D.M., Gobron, N., Willett, K.M. (Eds.), State of the Climate in 2017, Ch. 2 Global Climate 99. Bulletin of the American Meteorological Society, pp. S46–S49 8.

EIA, 2017. International energy outlook 2017. U.S. Energy Information Administration. https://www.eia.gov/outlooks/ieo/pdf/0484(2017).pdf, Accessed date: 6 December 2018.

Etheridge, D.M., Steele, L.P., Langenfelds, R.L., Francey, R.J., Barnola, J.M., Morgan, V.I., 1996. Natural and anthropogenic changes in atmospheric CO_2 over the last 1000 years from air in Antarctic ice and firn. J. Geophys. Res. 101 (D2), 4115–4128. http://doi.org/10.1029/95JD03410.

Everson, J.E., 1979. Regional variations in the lead isotopic characteristics of late Cenozoic basalts from the southwestern United States. Ph.D. dissertation. California Institute of Technology, Pasadena, pp. 464.

Galeczka, I., Wolff-Boenisch, D., Oelkers, E.H., Gislason, S.R., 2014. An experimental study of basaltic glass-H_2O-CO_2 interaction at 22 and 50 °C: Implications for subsurface storage of CO_2. Geochem. Cosmochim. Acta 126, 123–145. https://doi.org/j.gca.2013.10.044.

Garcia, B., Beaumont, V., Perfetti, E., Rouchon, V., Blanchet, D., Oger, P., Dromart, G., Huc, A.-Y., Haeseler, F., 2010. Experiments and geochemical modelling of CO_2 sequestration by olivine: Potential, quantification. Appl. Geochem. 25, 1383–1396. https://doi.org/10.1016/j.appgeochem.2010.06.009.

García del Real, P., Vishal, V., 2016. Mineral carbonation in ultramafic and basaltic rocks. In: Vishal, V., Singh, T.N. (Eds.), Geologic Carbon Sequestration: Switzerland. Springer International Publishing, pp. 213–229. https://doi.org/10.1007/978-3-319-27019-7_11.

Gislason, S.R., Wolff-Boenisch, D., Stefansson, A., Oelkers, E.H., Gunnlaugsson, E., Sigurdardottir, H., Sigfusson, B., Broecker, W.S., Matter, J., Stute, M., Axelsson, G., Fridriksson, T., 2010. Mineral sequestration of carbon dioxide in basalt: a preinjection overview of the CarbFix project. International Journal of Greenhouse Gas Control 4, 537–545.

Griffioen, J., 2017. Enhanced weathering of olivine in seawater: The efficiency as revealed by thermodynamic scenario analysis. Sci. Total Environ. 575, 536–544. https://doi.org/10.1016/j.scitotenv.2016.09.008.

Guha Roy, D., Vishal, V., Singh, T.N., 2016. Effect of carbon dioxide sequestration on the mechanical properties of Deccan basalt. Environmental Earth Science 75 (771), 13. https://doi.org/10.1007/s12665-016-5587-4.

Gysi, A.P., Stefánsson, A., 2011. CO_2-water-basalt interaction. Numerical simulation of low temperature CO_2 sequestration into basalts. Geochem. Cosmochim. Acta 75, 4728–4751. https://doi.org/10.1016/j.gca.2011.05.037.

Gysi, A.P., Stefánsson, A., 2012a. CO_2-water-basalt interaction. Low temperature experiments and implications for CO_2 sequestration into basalts. Geochem. Cosmochim. Acta 81, 129–152. https://doi.org/10.1016/j.gca.2011.12.012.

Gysi, A.P., Stefánsson, A., 2012b. Mineralogical aspects of CO_2 sequestration during hydrothermal basalt alteration – An experimental study at 75 to 250 °C and elevated pCO_2. Chem. Geol. 306–307, 146–159. https://doi.org/10.1016/j.chemgeo.2012.03.006.

Hartmann, D.L., Klein Tank, A.M.G., Rusticucci, M., Alexander, L.V., Brönnimann, S., Charabi, Y., Dentener, F.J., Dlugokencky, E.J., Easterling, D.R., Kaplan, A., Soden,

B.J., Thorne, P.W., Wild, M., Zhai, P.M., 2013. Observations: Atmosphere and Surface. In: Stocker, T.F., Qin, D., Plattner, G.-K., Tignor, M., Allen, S.K., Boschung, J., Nauels, A., Xia, Y., Bex, V., Midgley, P.M. (Eds.), Climate Change 2013: The Physical Science Basis. Contribution of Working Group I to the Fifth Assessment Report of the Intergovernmental Panel on Climate Change. Cambridge University Press, Cambridge, United Kingdom and New York, NY, USA.

Hellevang, H., Declercq, J., Aagaard, P., 2011. Why is dawsonite absent in CO_2 charged reservoirs? Oil & gas science and technology − Re. IFP Energies nouvelles 66, 119–135. https://doi.org/10.2516/ogst/2011002.

Hellevang, H., Miri, R., Haile, B.G., 2014. New insights into the mechanisms controlling the rate of crystal growth. Cryst. Growth Des. 14, 6451–6458.

Hellevang, H., Haile, B.G., Tetteh, A., 2017. Experimental study to better understand factors affecting the CO_2 mineral trapping potential of basalt. Greenhouse Gases Science and Technology 7, 143–157.

IPCC, 2014. In: Pachauri, R.K., Meyer, L.A. (Eds.), Climate Change 2014: Synthesis Report. Contribution of Working Groups I, II and III to the Fifth Assessment Report of the Intergovernmental Panel on Climate Change [Core Writing Team. IPCC, Geneva, Switzerland, pp. 151.

Johnson, N.C., Thomas, B., Maher, K., Rosenbauer, R.J., Bird, D., Brown Jr., G.E., 2014. Olivine dissolution and carbonation under conditions relevant for in situ carbon storage. Chem. Geol. 373, 93–105. https://doi.org/j.chemgeo.2014.02.026.

Kim, J., Lin, L.C., Swisher, J.A., Haranczyk, M., Smit, B., 2012. Predicting large CO_2 adsorption in aluminosilicate zeolites for post combustion carbon dioxide capture. J. Am. Chem. Soc. 134, 18940–18943.

Krajick, K., 2003. Killer lakes: Smithsonian 34, 46–50.

Kularatne, K., Sissmann, O., Kohler, E., Chardin, M., Noirez, S., Martinez, I., 2018. Simultaneous ex-situ CO_2 mineral sequestration and hydrogen production from olivine-bearing mine tailings. Appl. Geochem. 95, 195–205. https://doi.org/10.1016/j.apgeochem.2018.05.020.

Liu, H., Liu, B., Lin, L.C., Chen, G., Wu, Y., Wang, J., Gao, X., Lv, Y., Pan, Y., Zhang, X., Zhang, X., Yang, L., Sun, C., Smit, B., Wang, W., 2014. A hybrid absorption-adsorption method to efficiently capture carbon. Nat. Commun. 5 (5147), 7. https://doi.org/10.1038/ncomms6147.

Lum, C.C.L., Leeman, W.P., Foland, K.A., Kargel, J.A., Fitton, J.G., 1989. Isotopic variations in continental basaltic lavas as indicators of mantle heterogeneity: examples from the western U.S. cordillera. J. Geophys. Res. B 94, 7871–7884.

Mac Dowell, N., Fennell, P.S., Shah, N., Maitland, G.C., 2017. The role of CO_2 capture and utilization in mitigating climate change. Nat. Clim. Change 7, 243–249. https://doi.org/10.1038/NCLIMATE3231.

Mark, R.K., Lee Hu, C., Bowman, H.R., Asaro, F., McKee, E.H., Coats, R.R., 1975. A high $^{87}Sr/^{86}Sr$ mantle source for low alkali tholeiite, northern Great Basin. Geochem. Cosmochim. Acta 39, 1671–1678.

Mazzotti, M., Abanades, J.C., Allam, R., Lackner, K.S., Meunier, F., Rubin, W., Sanchez, J.C., Yogo, K., Sevenhoven, R., 2005. Mineral carbonation and industrial uses of carbon dioxide: Intergovernmental Panel on Climate Change, 2005, Carbon dioxide capture and storage, IPPC special report. www.ipcc.ch/activity/srccs/index.htm 320-338.

McGrail, B.P., Spane, F.A., Amonette, J.E., Thompson, C.R., Brown, C.F., 2014. Injection and monitoring at the Wallula basalt pilot project. Energy Procedia 63, 2939–2948. https://doi.org/10.1016/j.egypro.2014.11.316.

McGrail, B.P., Schaef, H.T., Spane, F.A., Cliff, J.B., Qafoku, O., Horner, J.A., Thompson, C.J., Owen, A.T., Sullivan, C.E., 2017. Field validation of supercritical CO_2 reactivity with basalt. Environ. Sci. Technol. Lett. 4, 6–10. https://doi.org/10.1021/acs.estlett.6b00387.

Middleton, R.S., Keating, G.N., Stauffer, P.H., Jordan, A.B., Viswanathan, H.S., Kang, Q.J., Carey, J.W., Mulkey, M.L., Sullivan, E.J., Chu, S.P., Esposito, R., Meckel, T.A., 2012. The cross-scale science of CO_2 capture and storage: From pore scale to regional scale. Energy Environ. Sci. 5, 7328–7345.

NV Energy, 2018. NV Energy-owned generating resources. https://www.nvenergy.com/about-nvenergy/our-company/power-supply, Accessed date: 4 December 2018.

Ormerod, D.S., 1988. Late- to post-subduction magmatic transitions in the western Great Basin, U.S.A. Ph.D. dissertation. Open University, Milton Keynes, UK, pp. 331.

Pan, S.-Y., Ling, T.-C., Park, A.-H.A., Chiang, P.-C., 2018. An overview: Reaction mechanisms and modelling of CO_2 utilization via mineralization. Aerosol and Air Quality Research 18, 829–848. https://doi.org/10.4209/aaqr.2018.03.0093.

Peduzzi, 2014. Sand, rarer than one thinks. United Nations Environmental Programme, pp. 15. https://na.unep.net/geas/archive/pdfs/GEAS_Mar2014_Sand_Mining.pdf.

Piers, J., Martins, F., Alvim-Ferraz, M., Simões, M., 2011. Recent developments on carbon capture and storage: an overview. Chem. Eng. Res. Des. 89, 1446–1460.

Price, J.G., Hess, R.H., Fitch, S., Faulds, J.E., Garside, L.J., Shevenell, L., Warren, S., 2005. Preliminary assessment of the potential for carbon dioxide sequestration in geological settings in Nevada. Nevada Bureau of Mines and Geology Report 51, 36.

Rackley, S.A., 2017. In: Carbon capture and storage, second ed. Butterworth-Heinemann/Elsevier, Oxford, UK, pp. 698.

Renforth, P., Pogge von Strandmann, P.A.E., Henderson, G.M., 2015. The dissolution of olivine added to soil: Implications for enhanced weathering. Appl. Geochem. 61, 109–118. https://doi.org/10.1016/j.apgeochem.2015.05.016.

Rezakazemi, M., Heydari, I., Zhang, Z., 2017. Hybrid systems: combining membrane and absorption technologies leads to more efficient acid gases (CO_2 and H_2S) removal from natural gas. Journal of CO_2 Utilization 18, 362–369. https://doi.org/10.1016/j.jcou.2017.02.006.

Rigopoulos, I., Petallidou, K.C., Vasiliades, M.A., Delimitis, A., Ioannou, I., Efstathiou, A.M., Kyratsi, T., 2015. Carbon dioxide storage in olivine basalts: Effect of ball milling process. Powder Technol. 273, 220–229. https://dx.doi.org/10.1016/j.powtec.2014.12.046.

Rigopoulos, I., Delimitis, A., Ioannou, I., Efstathiou, A.M., Kyratsi, T., 2018. Effect of ball milling on carbon sequestration efficiency of serpentinized peridotites. Miner. Eng. 120, 66–74. https://doi.org/10.1016/j.mineng.2018.02.011.

Roberts, R.J., 1964. Stratigraphy and structure of the Antler Peak Quadrangle, Humboldt and Lander Counties, Nevada. U.S. Geological Survey Professional Paper 459-A, pp. 93.

Rogers, K.L., Neuhoff, P.S., Pedersen, A.K., Bird, D.K., 2006. CO_2 metasomatism in a basalt-hosted petroleum reservoir, Nuussuaq, West Greenland. Lithos 92, 55–82.

Service, R.F., 2004. The carbon conundrum. Science 305, 962–963.

Sissman, O., Brunet, F., Martinez, I., Guyot, F., Verlaguet, A., Pinquier, Y., Daval, D., 2014. Enhanced olivine carbonation within a basalt as compared to single-phase experiments: reevaluating the potential of CO_2 mineral sequestration. Environ. Sci. Technol. 48, 5512–5519. https://doi.org/10.1021/es405508a.

Snæbjörnsdóttir, S.Ó., Oelkers, E.H., Mesfin, K., Sif Aradóttir, E., Dideriksen, K., Gunnarsson, I., Gunnlaugsson, E., Matter, J.M., Stute, M., Gislason, S.R., 2017. The chemistry and saturation states of subsurface fluids during the *in situ* mineralization of CO_2 and H_2S at the CarbFix site in SW-Iceland. International Journal of Greenhouse Gas Control 58, 87–102. https://doi.org/10.1016/j.ijggc.2017.01.007.

Snæbjörnsdóttir, S.Ó., Gislason, S.R., Galeczka, I.M., Oelkers, E.H., 2018. Reaction path modelling of *in-situ* mineralization of CO_2 at the CarbFix site at Hellisheidi, SW-Iceland. Geochem. Cosmochim. Acta 220, 348–366. https://doi.org/10.1016/j.gca.2017.09.053.

Speed, R.C., 1962. Scapolitized gabbroic complex, West Humboldt Range, Nevada. Ph.D. dissertation. Stanford University, Palo Alto, California, pp. 227.

Stewart, J.H., Carlson, J.E., 1978. Million-scale geologic map of Nevada. Nevada Bureau of Mines and Geology Map 57 scale 1:1,000,000.

Sturmer, D.M., La Pointe, D.D., Price, J.G., Hess, R.H., 2007. Assessment of the potential for carbon dioxide sequestration by reactions with rocks in Nevada. Nevada Bureau of Mines and Geology Report 52, 42.

Trask, N.J., 1969. Ultramafic xenoliths in basalt, Nye County, Nevada. U. S. Geological Survey Professional Paper 650-D, pp. D43–D48.

Wang, M., Wang, Z., Zhao, S., Wang, J., Wang, S., 2017. Recent advances on mixed matrix membranes for CO_2 separation. Chinese Journal of Chemical Engineering 25, 1581–1597. http://dx.dioi.org/10.1016/j.cjche.2017.07.006.

Wilshire, H.G., Schwarzman, E.C., Trask, N.J., 1972. Distribution of ultramafic xenoliths at 12 North American sites: U. S. Geological Survey Interagency Report: Astrogeology 42, 87.

Wolery, T.J., 1992. EQ3NR, a computer program for geochemical aqueous speciation-solubility calculations: theoretical manual, user's guide, and related documentation 7.0 Lawrence Livermore National Laboratory report no. UCRL-MA-110662 PT III.

Wolery, T.J., Daveler, S.A., 1992. EQ6, A computer program for reaction path modeling of aqueous geochemical systems: theoretical manual, user's guide, and related documentation. Lawrence Livermore National Laboratory report no. UCRL-MA-110662 PT IV version 7.0.

Wolff-Boenisch, D., Galeczka, I.M., 2018. Flow-through reactor experiments on basalt-(sea)water-CO_2 reactions at 90°C and neutral pH. What happens to the basalt pore space under post-injection conditions? International Journal of Greenhouse Gas Control 68, 176–190. https://doi.org/10.1016/j.ijggc.2017.11.013.

Yarushina, V.M., Bercovici, D., 2013. Mineral carbon sequestration and induced seismicity. Geophys. Res. Lett. 40, 814–818. https://doi.org/10.1002/grl.50196.

Zhang, Z., Borhani, T.N.G., El-Naas, M.H., 2018a. Carbon capture. In: Dincer, I., Colpan, C.O., Kizilkan, O. (Eds.), Exergetic, energetic and environmental dimensions. Elsevier, pp. 997–1016.

Zhang, Z., Cai, J., Chen, F., Li, H., Zhang, W., Qi, W., 2018b. Progress in enhancement of CO_2 absorption by nanofluids: a mini review of mechanisms and current status. Renew. Energy 118, 527–535.

Zhang, Z., Li, Y., Zhang, W., Wang, J., Soltanian, M.R., Olabi, A.G., 2018c. Effectiveness of amino acid salt solutions in capturing CO_2: a review. Renew. Sustain. Energy Rev. 98, 179–188. https://doi.org/10.1016/j.rser.2018.09.019.

Zhang, Z., Chen, F., Rezakazemi, M., Zhang, W., Lu, C., Chang, H., Quan, X., 2018d. Modeling of a CO_2-piperazine-membrane absorption system. Chem. Eng. Res. Des. 131, 375–384. https://doi.org/10.1016/j.cherd.2017.11.024.

Zhao, X., Deng, H., Wang, W., Han, F., Li, C., Zhang, H., Dai, Z., 2017. Impact of naturally leaking carbon dioxide on soil properties and ecosystems in the Qinghai-Tibet plateau. Sci. Rep. 7 (3001), 11. https://doi.org/10.1038/s41598-017-02500-x.

Zoback, M.D., Gorelick, S.M., 2012. Earthquake triggering and large-scale geologic storage of carbon dioxide. Proc. Natl. Acad. Sci. Unit. States Am. 109, 10164–10168. https://doi.org/10.1073/pnas.1202473109.